Supporting Information for Biomarker Displacement Activation: a General Host-Guest Strategy for Targeted Phototheranostics in Vivo

Jie Gao[†,#], Jun Li[‡,#], Wen-Chao Geng[†], Fang-Yuan Chen[†], Xingchen Duan[‡], Zhe Zheng[†], Dan Ding*[,‡], and Dong-Sheng Guo*[,†,§]

[†]College of Chemistry, State Key Laboratory of Elemento-Organic Chemistry, Key Laboratory of Functional Polymer Materials, Ministry of Education, Nankai University Tianjin 300071, P. R. China.

[‡]State Key Laboratory of Medicinal Chemical Biology, Key Laboratory of Bioactive Materials, Ministry of Education, and College of Life Sciences, Nankai University, Tianjin 300071, P. R. China.

[§]Collaborative Innovation Center of Chemical Science and Engineering, Nankai University Tianjin 300071, P. R. China.

Table contents

1 General methods and materials

1.1 Materials. All the reagents and solvents were commercially available and used as received unless otherwise specified purification. Eosin Y (EY), rose bengal (RB), adenosine triphosphate (ATP) and 2,7-dichlorofluorescein diacetate (DCFH-DA) were purchased from Sigma-Aldrich. Fetal bovine serum (FBS) and Dulbecco's modified eagle medium (DMEM) were purchased from Thermo Fisher Scientific. 5, 10, 15, 20-Tetrakis-(4-sulfonatophenyl)-porphyrin (TPPS) was purchased from TCI. Al(III) phthalocyanine chloride tetrasulfonic acid ($AlPcS_4$) was obtained from Frontier Scientific. The mouse serum was purchased from Manuik. 4-(Dodecyloxy)benzamido-terminated methoxy poly(ethylene glycol) (PEG-12C) was synthesized according to the previous literature.[1]

1.2 Samples. The HEPES buffer solution of pH 7.4 was prepared by dissolving 2.38 g of 4-(2-hydroxyethyl)piperazine-1-ethanesulfonic acid (HEPES) in approximate 900 mL double-distilled water. Titrate to pH 7.4 at 25 °C with NaOH and make up volume to 1000 mL with double-distilled water. The pH value of the buffer solution was then verified on a pH-meter calibrated with three standard buffer solutions. The samples for scanning electron microscopy (SEM) measurement were prepared by dropping the solution onto a silicon wafer which was then dried in air. Samples were coated with gold for two minutes using a gold sputter coater JFC-1600 prior to SEM experiments to improve surface conductivity. The sample for transmission electron microscopy (TEM) measurement was prepared by dropping the solution onto a copper grid without staining. The grid was then air-dried.

1.3 Instruments. ^{1}H and ^{13}C NMR data were recorded on a Bruker AV400 spectrometer. Mass spectra were performed on a Varian 7.0T FTICR-MS (ESI-FTMS). The sample solutions for dynamic light scattering (DLS) measurements were examined on a laser light scattering spectrometer (NanoBrook 173plus and Brookhaven ZetaPals/BI-200SM) equipped with a digital correlator at 659 nm and 532 nm at a scattering angle of 90°, respectively. SEM images were recorded on a JSM-7500F scanning electron microscope. The TEM sample was examined by a high-resolution TEM (Tecnai G2 F20 microscope, FEI) equipped with a CCD camera (Orius 832, Gatan). Steady-state fluorescence measurements were recorded in a

conventional quartz cuvette (light path 10 mm) on a Cary Eclipse equipped with a Cary single-cuvette peltier accessory. The fluorescence lifetimes were measured by time-correlated single photon counting on a FLS920 instrument (Edinburg Instruments Ltd., Livingstone, UK) with a H_2 pulse lamp. UV-Vis spectra were recorded in a quartz cuvette (light path 10 mm) on a Shimadzu UV-2450 UV-Vis spectrophotometer equipped with a dual cuvette peltier accessory and a temperature controller (TCC-240A). The cells were observed by confocal laser scanning microscopy (CLSM) (Leica TCS SP3, Germany).

1.4 Preparation of the pegylated GC5A-12C nanocarrier. GC5A-12C and PEG-12C (molar ratio 1:1) were dissolved in mixture solution of methanol and chloroform (1:1, v/v). After removal of solvent under reduced pressure for 12 h, the residue was hydrated in HEPES buffer (10 mM, pH = 7.4) by sonication at 80 °C for 3–5 h.

1.5 Fluorescence quantum yield and $^1O_2$ generation measurements. The fluorescence quantum yields were determined using the eq. 1:

$$\Phi_{\text{Fluo}} = \Phi_{\text{Fluo}}^{\text{Std}} \frac{I}{I^{\text{Std}}} \frac{1-10^{-A^{\text{Std}}(\lambda_{\text{ex}})}}{1-10^{-A(\lambda_{\text{ex}})}} \frac{n^2}{n_{\text{Std}}^2} \qquad (1)$$

where Φ_{Fluo} is fluorescence quantum yield, n is the refractive index, I is the integrated fluorescence intensity and A is the absorbance at the excitation wavelength. The superscript "Std" refers to the sample of the standard.[2] In this work, the fluorescence quantum yield of each PS/GC5A-12C uses the PS itself as a standard.[3]

The $^1O_2$ generation was measured by the *p*-nitroso-N,N-dimethylaniline (RNO, $^1O_2$ sensor) / histidine assay based on the oxidation of histidine by $^1O_2$ and the subsequent reaction of the oxidized histidine with RNO as previously described.[4, 5] In brief, RNO (50 μM) and histidine (10 mM) were mixed with $AlPcS_4$ (or other PSs) in the absence and presence of the GC5A-12C nanocarrier, and upon addition of ATP (10 nM and 100 μM, respectively. Then the mixed solutions were illuminated by a xenon lamp (filtered to remove light with λ < 400 nm) and the UV absorption at 440 nm was detected immediately every several minutes to monitor the consumption of RNO. Control experiments, only having RNO and histidine, were run by repeating the

measurements. Meanwhile, all samples were stable in darkness and no degradation of RNO was observed. The absorbance changes at 440 nm were then plotted as a function of irradiation time (0–5 min) and the quantum yield of $^1O_2$ generation (Φ_Δ) was calculated using PS itself as the standard (Φ_Δ^{Std}) according to eq. 2:

$$\Phi_\Delta = \Phi_\Delta^{Std} \frac{R}{R^{Std}} \frac{\int_{\lambda_{ex}} \left[1-10^{-A^{Std}(\lambda_{ex})}\right] d\lambda_{ex}}{\int_{\lambda_{ex}} \left[1-10^{-A(\lambda_{ex})}\right] d\lambda_{ex}} \qquad (2)$$

where Φ_Δ^{Std} is the $^1O_2$ quantum yield for the standard PS; R denotes the slope of a plot of the change in absorbance for RNO at 440 nm *vs.* the irradiation time. A is the absorbance at the excitation wavelength.

1.6 Calculation of rate constants of fluorescence emission, intersystem crossing (ISC) and photoinduced electron transfer (PET).[2] The lifetime of the fluorophore in the absence of non-radiative processes is called the intrinsic or natural lifetime, and is given by eq. 3:

$$\tau_n = \tau_0 / \Phi_{Fluo} \qquad (3)$$

where τ_n and τ_0 are the natural lifetime and measured lifetime of the fluorophore. Hence, the fluorescence emission rate constant (k_{Fluo}) can be deduced from eq. 4:

$$k_{Fluo} = 1/\tau_n \qquad (4)$$

The PET rate constant (k_{PET}) can be estimated utilizing eq. 5:

$$k_{PET} = \frac{1}{\tau_0}\left(\frac{\Phi_{Fluo}}{\Phi} - 1\right) \qquad (5)$$

where Φ is the fluorescence quantum yields of free fluorophore and the complex.

The ISC rate constant (k_{ISC}) can be deduced by eq. 6:

$$k_{ISC} = \Phi_T / \tau_0 \qquad (6)$$

where Φ_T is the triplet state quantum yield of the fluorophore. Herein, the Φ_T value of $AlPcS_4$ is 0.27 according to previous literature.[6]

1.7 Displacement release of PSs from the PS/GC5A-12C nanoparticles triggered by ATP and other components in blood. Various representative components of blood were added to the PS/GC5A-12C nanoparticles (2.0/2.0 μM) in HEPES buffer

(10 mM, pH = 7.4) at 25 °C and stirred for 30 min to monitor the fluorescence intensity of PS, where the fluorescence of PS alone as control. Condition: ATP 0.4 μM, adenosine diphosphate (ADP) 0.1 μM, adenosine monophosphate (AMP) 10 nM, nicotinamide adenine dinucleotide (NAD) 24 μM, glutamine 0.5 mM, alanine 0.4 mM, valine 0.2 mM, glycine 0.3 mM and lysine 0.2 mM; phosphate 0.8 mM, chloride 95 mM, bovine serum albumin (BSA) 10 μg/mL, glutathione 8.0 μM, creatinine 80 μM and glucose 5.0 mM. The concentrations of all above components refer to their concentrations in human blood.[7-11]

1.8 In vitro cytotoxicity assay of the GC5A-12C nanocarrier. Cell culture: Murine 4T1 breast cancer cells were incubated in DMEM medium with 10% FBS and 1% penicillin streptomycin at 37 °C in a humidified atmosphere containing 5% CO_2. Before experiments, the cells were pre-cultured until confluence was reached.

The cytotoxicity of the GC5A-12C nanocarrier against 4T1 cancer cells was evaluated by 3-(4,5-dimethylthiazol-2-yl)-2,5-diphenyl tetrazolium bromide (MTT) assay. In brief, 4T1 cells were seeded in 96-well plates at an appropriate density of 5×10^3 cells per well, respectively. After adherence, the cells were treated with the GC5A-12C nanocarrier with different concentrations ranging from 0 to 20 μM based on the GC5A-12C unit. After incubation for 6 h, the culture medium was replaced with fresh medium. The cells without any treatment were used as the control. Then, 100 μL of MTT solution (0.5 mg/mL) was added to each well and incubated for 4 h. Thereafter, the medium was removed and 100 μL of DMSO was added, followed by gently shaking for 10 min. The absorbance was measured at 490 nm using a microplate reader (Bio-Rad, iMark, USA). The relative cell viability was calculated as: cell viability = $(OD_{490\ (samples)}/OD_{490\ (control)}) \times 100\%$, where $OD_{490\ (control)}$ was obtained in the absence of GC5A-12C, and $OD_{490\ (samples)}$ was obtained in the presence of GC5A-12C. Each value was averaged from three independent experiments.

1.9 ATP-dependent $AlPcS_4$ release in cancer cells. 4T1 cells (1×10^5 cells per well) were seeded and cultured in confocal imaging chambers. After culture for 36 h, the cells were incubated with the $AlPcS_4$/GC5A-12C nanoparticle (10/10 μM) for 6 h at

37 °C. After washing the cells by PBS three times, the fluorescence of $AlPcS_4$ in the cells was detected using CLSM. Sodium azide (NaN_3) and Ca^{2+} were used to inhibit and promote ATP production in the cancer cells, respectively.[12,13] After cell incubation with 5 mM of Ca^{2+} or 10 mM of NaN_3 at 37 °C for 2 h, the excessive Ca^{2+} or NaN_3 were removed and the cells were incubated with the $AlPcS_4$/GC5A-12C nanoparticle (10/10 μM) for additional 6 h. After washing the cells by PBS three times, the fluorescence of $AlPcS_4$ in the cells was detected using CLSM. The laser excitation of 633 nm was used with a collection of $AlPcS_4$ fluorescence signal in the range of 660–700 nm.

1.10 Intracellular $^1O_2$ detection. The generation of intracellular $^1O_2$ was measured by CLSM using DCFH-DA as the $^1O_2$ indicator. After treating 4T1 cells with the $AlPcS_4$/GC5A-12C nanoparticle (10/10 μM) for 6 h in the dark, the culture media were removed and DCFH-DA was added (final concentration 10 μM) and incubated for 30 min. Subsequently, the cells were washed with PBS and further illuminated with a laser (660 nm, 300 $mW \cdot cm^{-2}$) for 3 min, followed by imaging with CLSM. Excitation of DCF was performed with a laser at 488 nm and emission spectrum was collected using a wavelength range of 510–540 nm. Alternatively, before treatment with the $AlPcS_4$/GC5A-12C nanoparticle, the cells were pre-treated with *N*-acetylcysteine (1.0 mM) for 2 h. In addition, the $AlPcS_4$/GC5A-12C nanoparticle-treated cells without laser irradiation, the cells with only pure laser irradiation, and the cells without any treatment were used as controls.

1.11 Intracellular photodynamic therapy (PDT). The 4T1 cancer cells were treated with the $AlPcS_4$/GC5A-12C nanoparticle (0–20 μM in a 1:1 molar ratio) in the dark. After incubation for 6 h, the culture medium was replaced with fresh medium. The cells were irradiated with 660 nm laser for 3 min at a power intensity of 300 $mW \cdot cm^{-2}$. Then, the cell viability was evaluated by MTT assay. As the control, the cytotoxicity of $AlPcS_4$/GC5A-12C in the dark was also evaluated. Each value was averaged from three independent experiments.

1.12 In vivo fluorescence imaging and antitumour study. For animals and tumour model, all animal studies were performed in compliance with the guidelines set by Tianjin Committee of Use and Care of Laboratory Animals and the overall project

protocols were approved by the Animal Ethics Committee of Nankai University. Female BALB/c nude mice (5–6 weeks old) and female BALB/c mice (5–6 weeks old) were bought from Vital River Laboratory Animal Technology (Beijing, China). Female BALB/c nude mice were used for in vivo fluorescence imaging and female BALB/c mice were used for animal treatment experiment. To establish the xenograft 4T1 tumour-bearing mouse model, 1×10^7 4T1 cancer cells were injected subcutaneously into the right axillary space of the mouse. The mice with tumour volumes at around 100 mm^3 were used subsequently.

In vivo fluorescence imaging: The 4T1 tumour-bearing mice were intravenously administrated with 200 μL of $AlPcS_4$/GC5A-12C nanoparticle suspension (containing $AlPcS_4$: 1.34 $mg\cdot kg^{-1}$). Then the mice were anesthetized and imaged *via* a CRI Maestro whole-animal imaging system (Caliper Life Sciences, MA, USA) at 1, 4, 6, 8 and 24 h post-injection. The excitation wavelength was 630 nm and in vivo spectral imaging from 650 to 750 nm (with 10 nm steps) was carried out. For the ex vivo tissues distribution study, the mice were sacrificed after 6 h injection, and tumour as well as major organs (spleen, kidney, lung, liver and heart) were collected and subjected for ex vivo imaging.

For antitumour study, the tumour-bearing mice were randomly divided into 6 groups (5 mice per group): 1) "Saline", 2) "Saline 660 nm", 3) "$AlPcS_4$" 4) "$AlPcS_4$ 660 nm", 5) "$AlPcS_4$/GC5A-12C", and 6) "$AlPcS_4$/GC5A-12C 660 nm". For "Saline", "$AlPcS_4$", and "$AlPcS_4$/GC5A-12C" groups, 4T1 tumour-bearing mice were intravenously administrated with saline, free $AlPcS_4$ (1.34 $mg\cdot kg^{-1}$), and the $AlPcS_4$/GC5A-12C nanoparticle (at dose of $AlPcS_4$ 1.34 $mg\cdot kg^{-1}$), respectively, on day 0. For "Saline 660 nm", "$AlPcS_4$ 660 nm", and "$AlPcS_4$/GC5A-12C 660 nm" cohorts, after injecting with saline, free $AlPcS_4$ (1.34 $mg\cdot kg^{-1}$), and the $AlPcS_4$/GC5A-12C nanoparticle (at dose of $AlPcS_4$ 1.34 $mg\cdot kg^{-1}$), respectively, *via* the tail vein on day 0, the mice were irradiated with 660 nm laser (300 $mW\cdot cm^{-2}$) for 5 min at 6 h and 24 h post-injection, respectively. The mice weight and tumour size were measured every other day for 16 days. Tumour size was measured by a caliper and tumour volume was calculated using the following formula: $V = W^2 \times L/2$, where

W and *L* were the shortest and longest diameters of tumours, respectively. Relative tumour size was calculated as V/V_0 (V_0 was the initial tumour volume). On day 16, all mice were sacrificed and the tumours were excised and weighed.

1.13 In vivo histological analysis. On day 16, the tumour tissues and the main organs (spleen and kidney) of the mice in the different groups were collected and fixed in 4% paraformaldehyde, and then, paraffin embedded sectioning was conducted for histological hematoxylin and eosin (H&E) staining. The slices were examined by a digital microscope (Leica Q Win). For proliferating cell nuclear antigen (PCNA) staining, formalin-fixed tumour and organs samples were sliced and used for confocal immunofluorescent analysis using PC10 Mouse mAb (#2586, Cell Signaling Technology) following the supplier's protocol. For the terminal deoxynucleotidyl transferased dUTP nick end labeling (TUNEL) apoptosis staining, the fixed tumour sections were determined following manual instruction of *in situ* Cell Death Detection Kit (Roche Applied Science). Hoechst 33342 was used for nuclear counterstaining.

1.14 Statistical analysis. Quantitative data were expressed as means (standard deviation). ANOVA and Student's t test were utilized for statistical analyses.

2 Syntheses of GC5A-12C and GC5A-6C

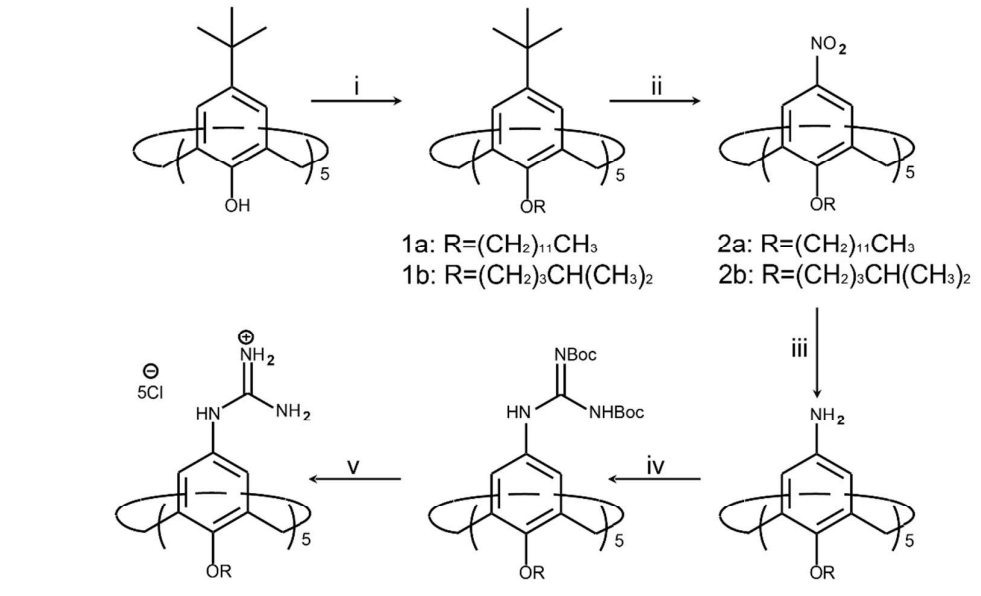

Scheme S1. Synthetic routes of **GC5A-12C** and **GC5A-6C**. (i) K_2CO_3, RBr, CH_3CN, reflux; (ii) HNO_3, AcOH, dry CH_2Cl_2, r.t.; (iii) $SnCl_2{\cdot}2H_2O$, C_2H_5OH/AcOEt (1:1, v:v), reflux; (iv) 1,3-bis(tert-butoxycarbonyl)-2-methyl-2-thiopseudourea, Et_3N, $AgNO_3$, dry CH_2Cl_2, r.t.; (v) $SnCl_4$, AcOEt, r.t.

Compound 1a and **GC5A-6C** were synthesized and purified according to the procedure reported previously. [14-16]

Compound 2a: To a solution of **1a** (3.97 g, 2.4 mmol) in dry CH_2Cl_2 (119 mL) and CH_3COOH (34.28 mL), HNO_3 (10.28 mL) was added gradually and the mixture was stirred for about 1–4 h at room temperature. The color of the mixture changed from dark purple to orange. Then water (250 mL) was added into the reaction mixture and followed by stirring for 30 min. The mixture was washed with saturated Na_2CO_3, brine and water. After drying with anhydrous Na_2SO_4, the solvent was removed in vacuo. The residue was recrystallized from CH_2Cl_2/CH_3OH to obtain yellow solid **2a** (1.71g, 45%).

^{1}H NMR (400 MHz, $CDCl_3$, δ): 7.85 (s, 10H, ArH), 4.59 (d, J = 14.74 Hz, 5H, Ar-CH_2-Ar), 3.87 (t, J = 7.52 Hz, 10H, CH_2-O-Ar), 3.55 (d, J = 14.74 Hz, 5H, Ar-CH_2-Ar), 1.89 (m, 10H, -CH_2-CH_2-O-Ar), 1.31 (m, 90H, alkyl CH_2), 0.91 (t, J = 6.60 Hz, 15H, -CH_3).

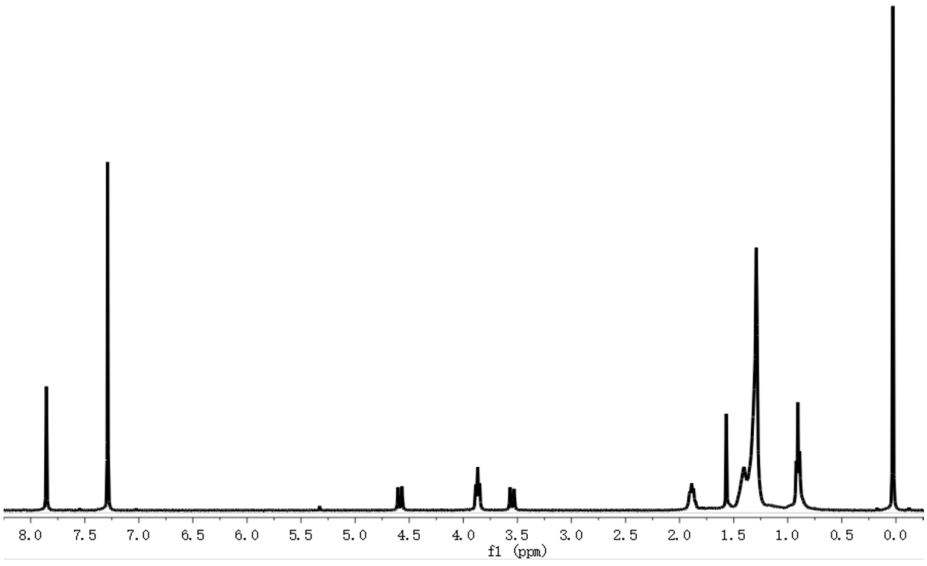

Figure S1. ^{1}H NMR spectrum of **2a** in $CDCl_3$, 400 MHz, 25 °C.

Compound 3a: To a solution of **2a** (0.38 g, 0.24 mmol) in dry C_2H_5OH/AcOEt (50 mL/50 mL), $SnCl_2{\cdot}2H_2O$ (0.15 g, 0.67 mmol) was added and the mixture was refluxed for 48 h. Then the mixture was pour into ice water. After all the ice melt, NaOH was added to the mixture to adjust the pH to 8.0. Dichloromethane was added and the mixture was stirred overnight at room temperature. The solution was washed by water for three times. After drying with anhydrous Na_2SO_4, the solvent was removed in vacuo to obtain white solid **3a** (0.24 g, 69%).

^{1}H NMR (400 MHz, $CDCl_3$, δ): 6.30 (s, 10H, ArH), 4.36 (d, J = 14.08 Hz, 5H, Ar-CH_2-Ar), 3.67 (t, J = 7.51 Hz, 10H, CH_2-O-Ar), 3.11 (d, J = 14.08 Hz, 5H, Ar-CH_2-Ar), 1.81 (m, 10H, -CH_2-CH_2-O-Ar), 1.28 (m, 90H, alkyl CH_2), 0.88 (t, J = 6.21 Hz, 15H, -CH_3).

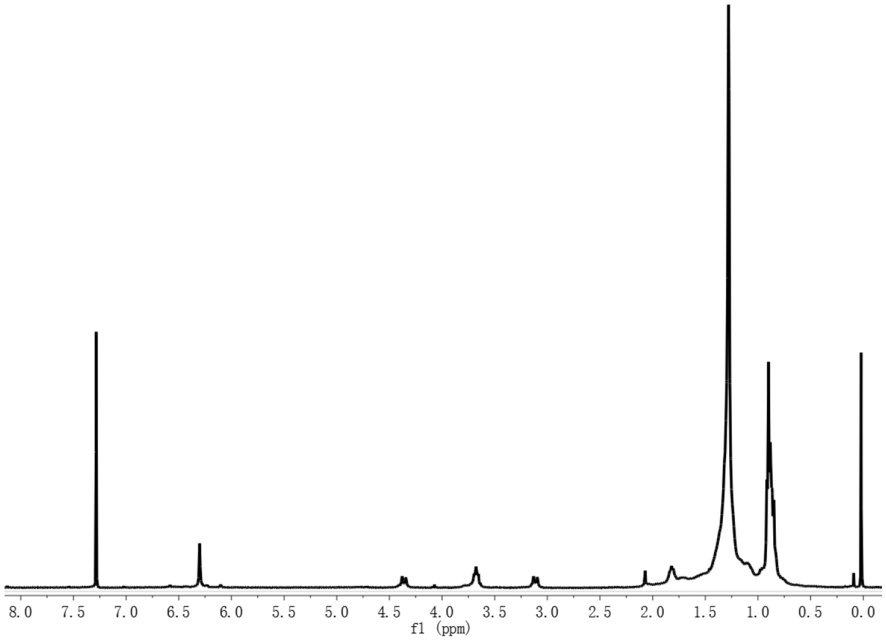

Figure S2. ^{1}H NMR spectrum of **3a** in $CDCl_3$, 400 MHz, 25 °C.

Compound 4a: To a solution of **3a** (0.32 g, 0.22 mmol) in dry CH_2Cl_2 (25 mL), 1,3-bis(tert-butoxycarbonyl)-2-methyl-2-thiopseudourea (0.33 g, 1.12 mmol), $AgNO_3$ (0.20 g, 1.19 mmol) and Et_3N (0.17 mL) were added and the mixture was stirred for

48 h at room temperature. The solvent was evaporated under reduced pressure and the residue was purified by column chromatography on silica gel to obtain a pale white powder **4a** (0.28 g, 48 %).

^{1}H NMR (400 MHz, $CDCl_3$, δ): 11.63 (s, 5H, NH), 9.87 (s, 5H, NH), 7.15 (s, 10H, ArH), 4.52 (d, J = 13.56 Hz, 5H, Ar-CH_2-Ar), 3.73 (t, J = 7.58 Hz, 10H, CH_2-O-Ar), 3.30 (d, J = 13.62 Hz, 5H, Ar-CH_2-Ar), 1.94 (m, 10H, -CH_2-CH_2-O-Ar), 1.46 (s, 90H, Bu^t), 1.28 (m, 90H, alkyl CH_2), 0.88 (t, J = 6.18 Hz, 15H, -CH_3).

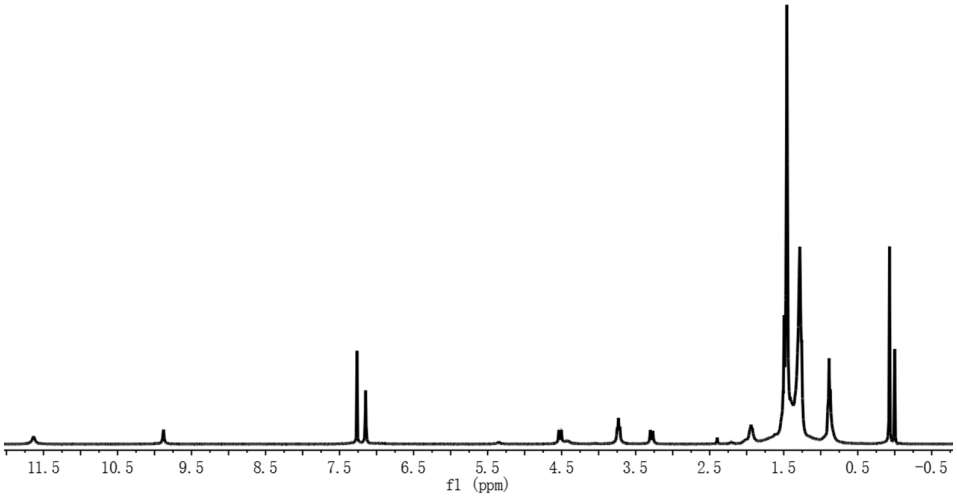

Figure S3. ^{1}H NMR spectrum of **4a** in $CDCl_3$, 400 MHz, 25 °C.

Compound GC5A-12C: $SnCl_4$ (0.2 mL) was added to a solution of **4a** (0.08 g, 0.03 mmol) in 20 mL of ethyl acetate. The mixture was stirred for 3 h at room temperature and the solvent evaporated under reduce pressure. The residue was dissolved in CH_3OH, then large amounts of diethyl ether was added to obtain white precipitations **GC5A-12C** (0.04 g, 72%).

^{1}H NMR (400 MHz, CD_3OD, δ): 6.91 (s, 10H, ArH), 4.51 (d, J = 13.86 Hz, 5H, Ar-CH_2-Ar), 3.81 (t, J = 7.48 Hz, 10H, CH_2-O-Ar), 3.38 (d, J = 13.63 Hz, 5H, Ar-CH_2-Ar), 1.93 (m, 10H, -CH_2-CH_2-O-Ar), 1.22 (m, 90H, alkyl CH_2), 0.81 (t, J = 6.07 Hz, 15H, -CH_3).

^{13}C NMR (100 MHz, CD_3OD, δ): 156.65, 154.70, 135.57, 129.45, 126.46, 74.51, 31.86, 30.38, 30.22, 30.01, 29.88, 29.74, 29.35, 26.41, 22.46, 13.13.

ESI-FTMS *m/z*: $[M + H - 5HCl]^+$ calcd. for $C_{100}H_{166}N_{15}O_5^+$ 1658.3224, found 1658.3188.

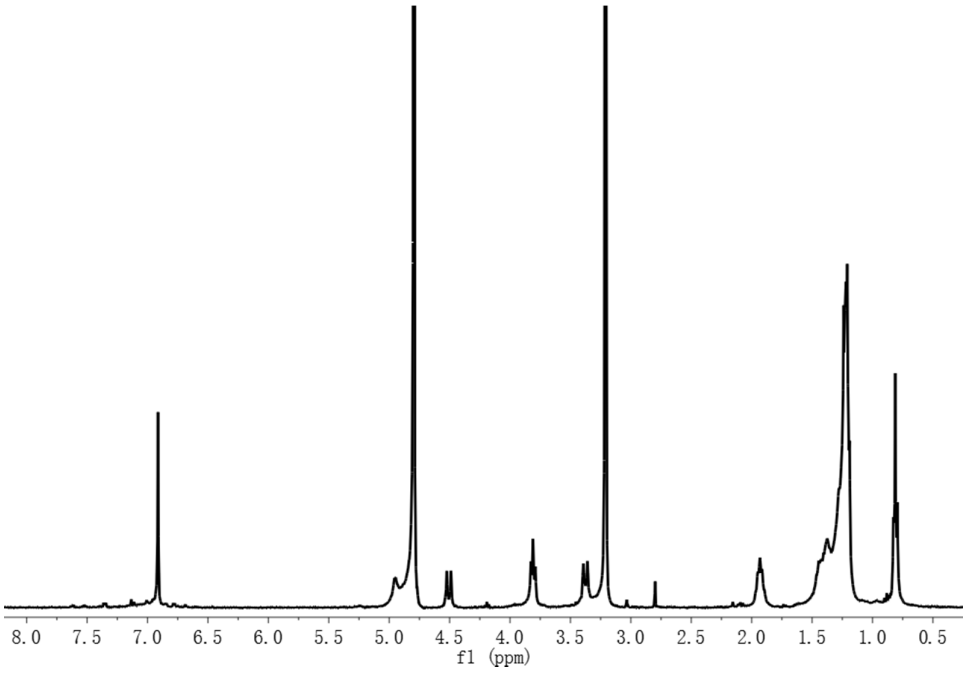

(a)

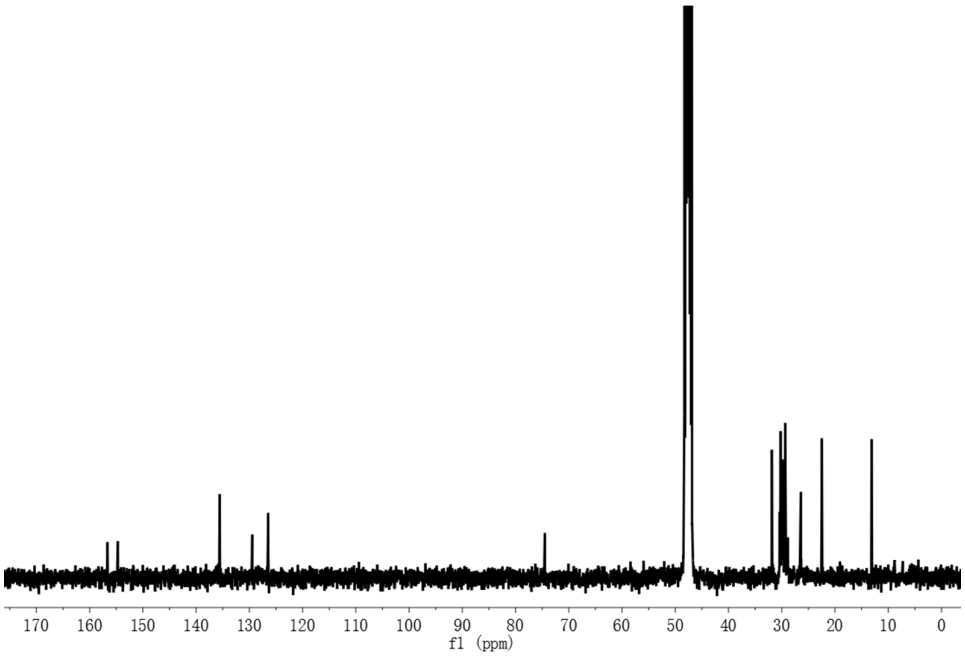

(b)

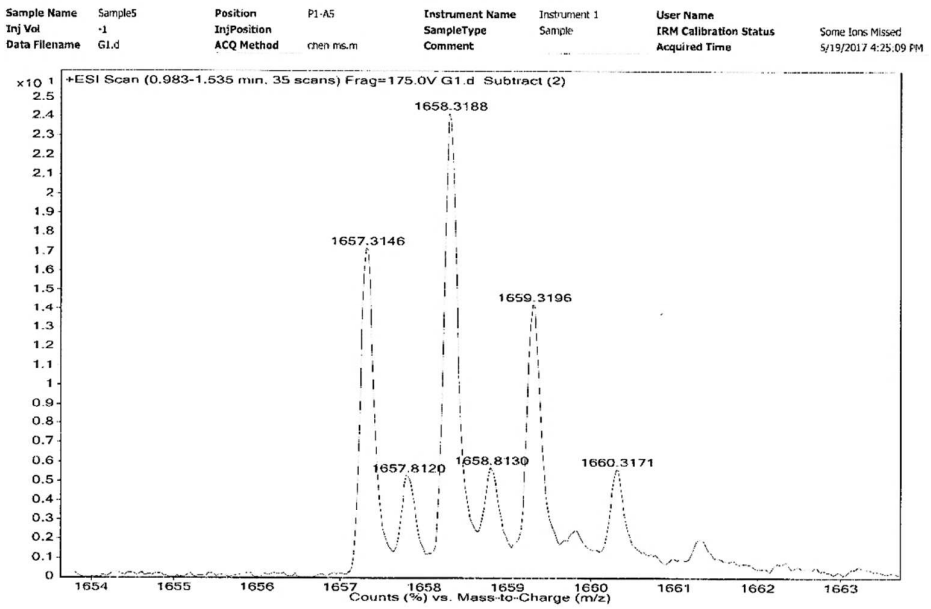

(c)

Figure S4. (a) ^{1}H NMR spectrum of **GC5A-12C** in CD_3OD, 400 MHz, 25 °C, and (b) ^{13}C NMR spectrum of **GC5A-12C** in CD_3OD, 100 MHz, 25 °C, and (c) ESI-FTMS of **GC5A-12C**.

3 Supporting results and experimental raw data

3.1 Characterization of the pegylated GC5A-12C nanocarrier.

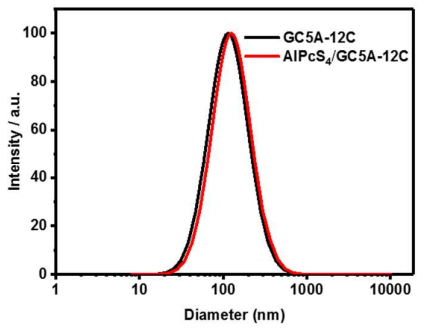

(a)

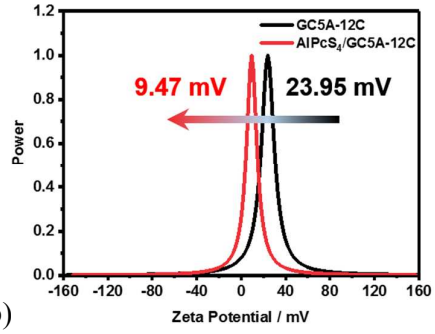

(b)

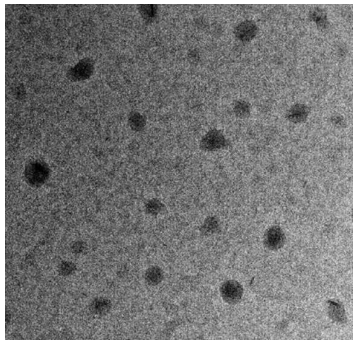

(c)

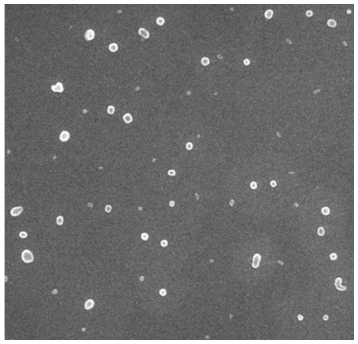

(d)

Figure S5. DLS (a) and zeta potential (b) results of the GC5A-12C nanocarrier (10

μM) in the absence (black) and presence of 10 μM $AlPcS_4$ (red) in HEPES buffer (10 mM, pH = 7.4) at 25 °C. TEM (c) and SEM (d) images of the GC5A-12C nanocarrier (GC5A-12C/PEG-12C = 50/50 μM in deionized water).

3.2 Binding affinities of GC5A-6C with PSs and ATP.

The complexation of GC5A-6C with PSs and ATP is so strong that the direct titrations cannot be fitted very well. In this context, we used the competitive fluorescence titration method to obtain their binding constants. Fluorescein (Fl) was employed as the reporter dye. The binding stoichiometry and the binding affinity (K_a) between GC5A-6C and Fl had been determined as 1:1 and $(5.0\pm1.0) \times 10^6$ M^{-1}, respectively.[16] The binding affinity of GC5A-6C with ATP had been obtained as $(4.7\pm1.4) \times 10^8$ M^{-1} using the competitive fluorescence titration method.[16]

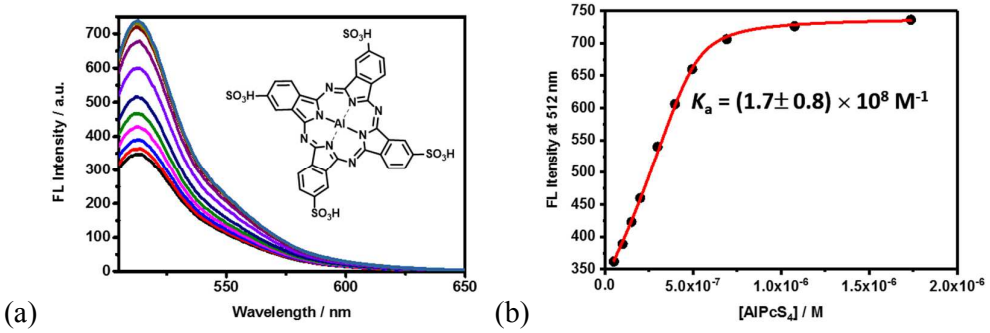

Figure S6. (a) Competitive fluorescence titration of GC5A-6C•Fl (0.5/0.5 μM) with $AlPcS_4$ (up to 1.7 μM), λ_{ex} = 500 nm. (b) The associated titration curve at λ_{em} = 512 nm and fit according to a 1:1 competitive binding model.

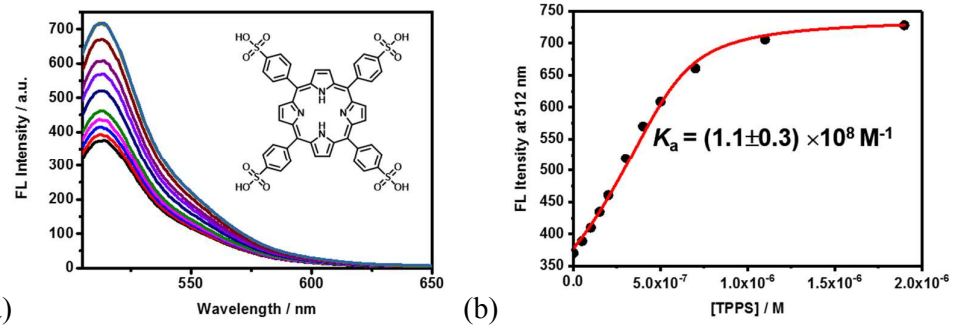

Figure S7. (a) Competitive fluorescence titration of GC5A-6C•Fl (0.5/0.5 μM) with TPPS (up to 1.9 μM), λ_{ex} = 500 nm. (b) The associated titration curve at λ_{em} = 512 nm and fit according to a 1:1 competitive binding model.

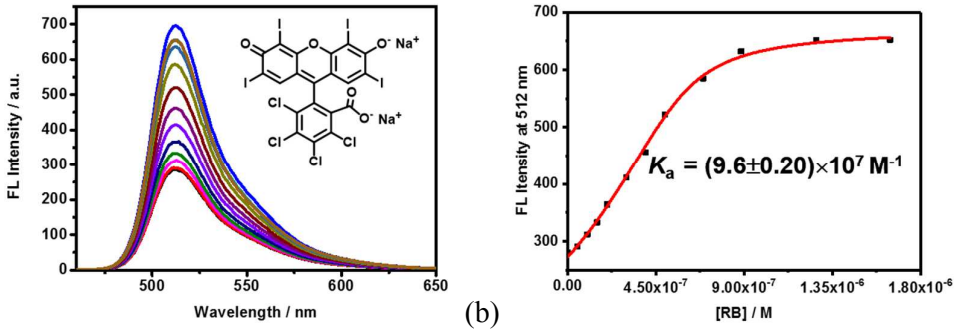

Figure S8. (a) Competitive fluorescence titration of GC5A-6C•Fl (0.6/0.5 μM) with RB (up to 1.6 μM), λ_{ex} = 450 nm. (b) The associated titration curve at λ_{em} = 512 nm and fit according to a 1:1 competitive binding model.

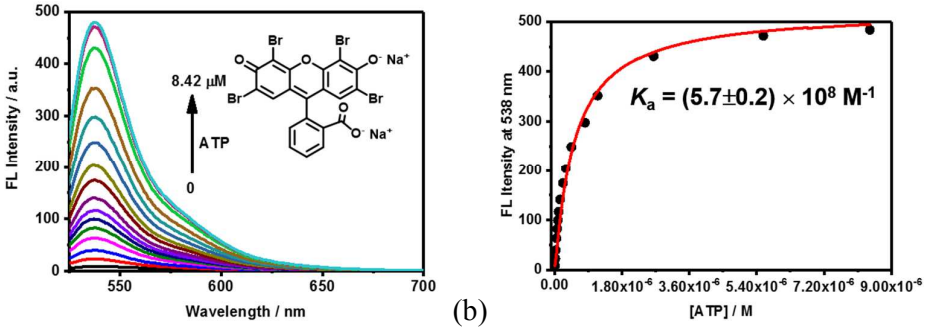

Figure S9. (a) Competitive fluorescence titration of GC5A-6C•EY (0.5/0.5 μM) with ATP (up to 8.4 μM), λ_{ex} = 517 nm. (b) The associated titration curve at λ_{em} = 538 nm and fit according to a 1:1 competitive binding model (K_{ATP} = 4.7 × 10^8 M^{-1}).

3.3 Fluorescence quenching of PSs by the complexation of GC5A-6C or GC5A-12C and the corresponding recovery by the displacement of ATP.

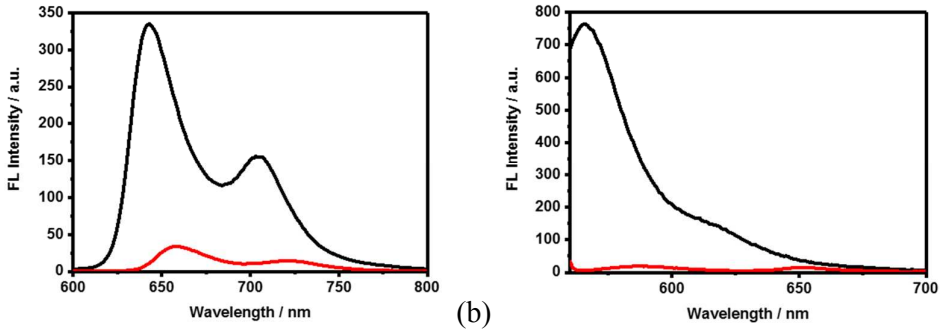

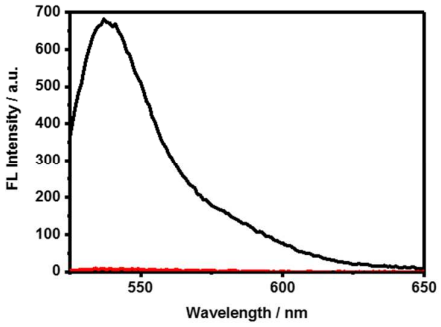

(c)

Figure S10. Fluorescence spectra of (a) TPPS (λ_{ex} = 412 nm, 0.5 μM), (b) RB (λ_{ex} = 550 nm, 0.5 μM) and (c) EY (λ_{ex} = 517 nm, 0.5 μM) in the absence (black) and presence (red) of GC5A-6C (0.5 μM) in 10 mM HEPES (pH = 7.4) at 25 °C.

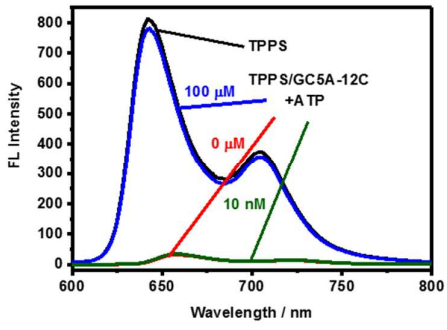

(a)

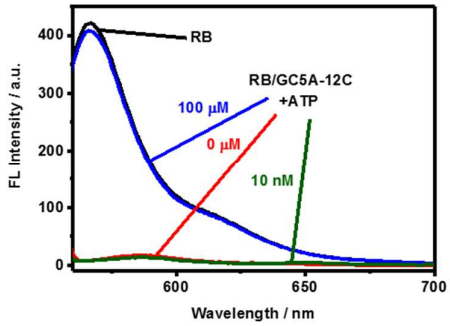

(b)

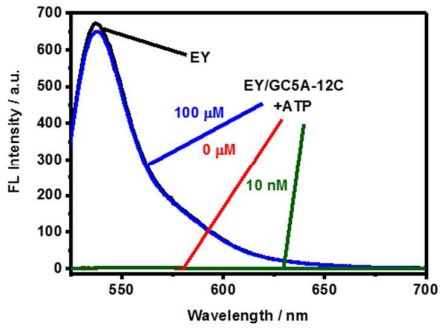

(c)

Figure S11. Fluorescence spectra of (a) TPPS (λ_{ex} = 412 nm, 2.0 μM), (b) RB (λ_{ex} = 550 nm, 2.0 μM) and (c) EY (λ_{ex} = 517 nm, 2.0 μM) in the absence (black) and presence of 2.0 μM GC5A-12C nanocarrier (red), and upon addition of 100 μM ATP (blue) and 10 nM ATP (green) in 10 mM HEPES (pH = 7.4) at 25 °C.

3.4 Photoactivity ($^1O_2$ generation) annihilation of PSs by the complexation of GC5A-12C and the corresponding recovery by the displacement of ATP.

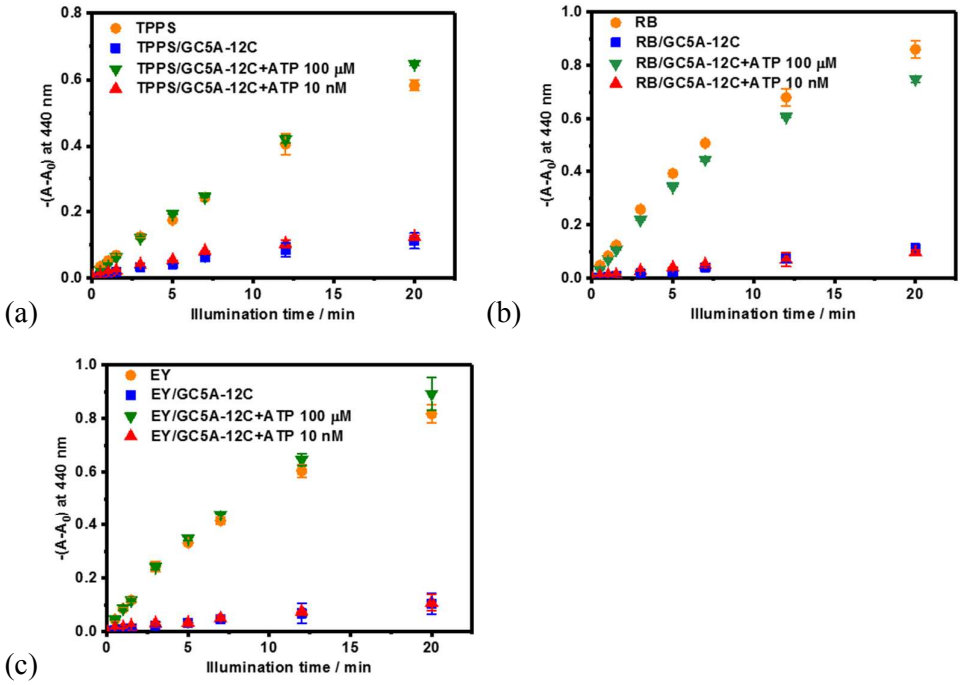

Figure S12. $^1O_2$ generation of (a) TPPS (2.0 μM), (b) RB (2.0 μM) and (c) EY (2.0 μM) in the absence (orange) and presence of 2.0 μM GC5A-12C nanocarrier (blue), and upon addition of 100 μM ATP (green) and 10 nM ATP (red) by using RNO as sensor (recording absorption changes at 440 nm) in 10 mM HEPES (pH = 7.4) at 25 °C.

Table S1. Fluorescence (Φ_{Fluo}) and $^1O_2$ (Φ_Δ) quantum yields of PSs (2.0 μM) in the absence and presence of 2.0 μM GC5A-12C nanocarrier in 10 mM HEPES buffer (pH = 7.4).

Analyte	**Φ_{Fluo} / %**	**Φ_Δ / %**
$AlPcS_4$	58[17]	22[17]
$AlPcS_4$/GC5A-12C	0.53±0.015	1.2±0.0058
TPPS	11[17]	62[17]
TPPS/GC5A-12C	1.2±0.020	8.2±0.042
RB	2[18]	75[18]
RB/GC5A-12C	0.11±0.010	5.9±0.015
EY	20[18]	55[18]
EY/GC5A-12C	2.1±0.067	6.9±0.032

3.5 Fluorescence lifetime measurements.

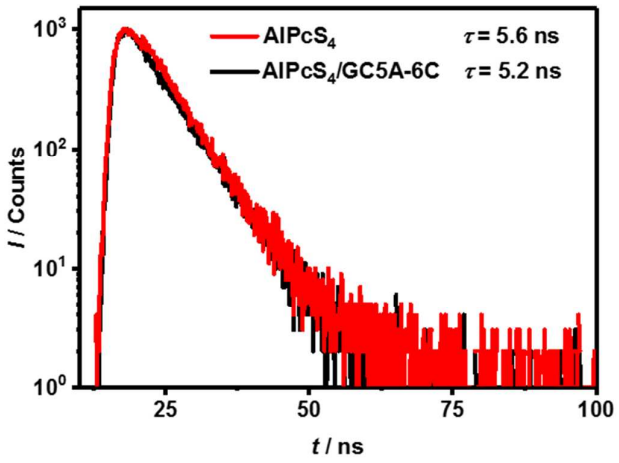

(a)

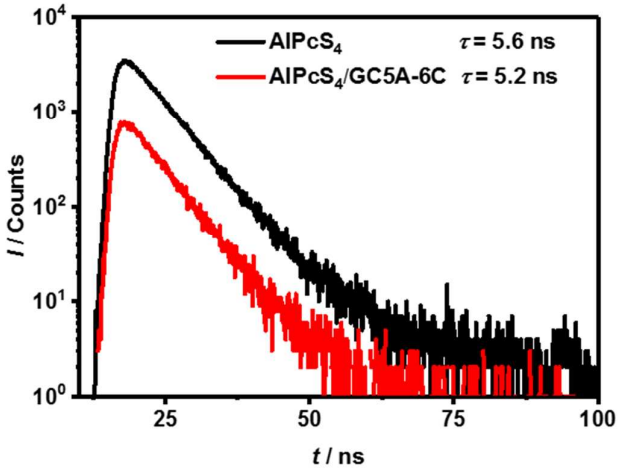

(b)

Figure S13. Fluorescence decay profiles of $AlPcS_4$ (2.0 μM, black) and $AlPcS_4$/GC5A-6C (2.0/1.6 μM, red) in HEPES buffer (10 mM, pH = 7.4), λ_{ex} = 660 nm. Conditions: (a) setting a specified number of photon counts as 1000; (b) setting specified time as 1 h.

3.6 Fluorescence recovery of the PS/GC5A-12C nanoparticles upon addition of ATP and other components in blood.

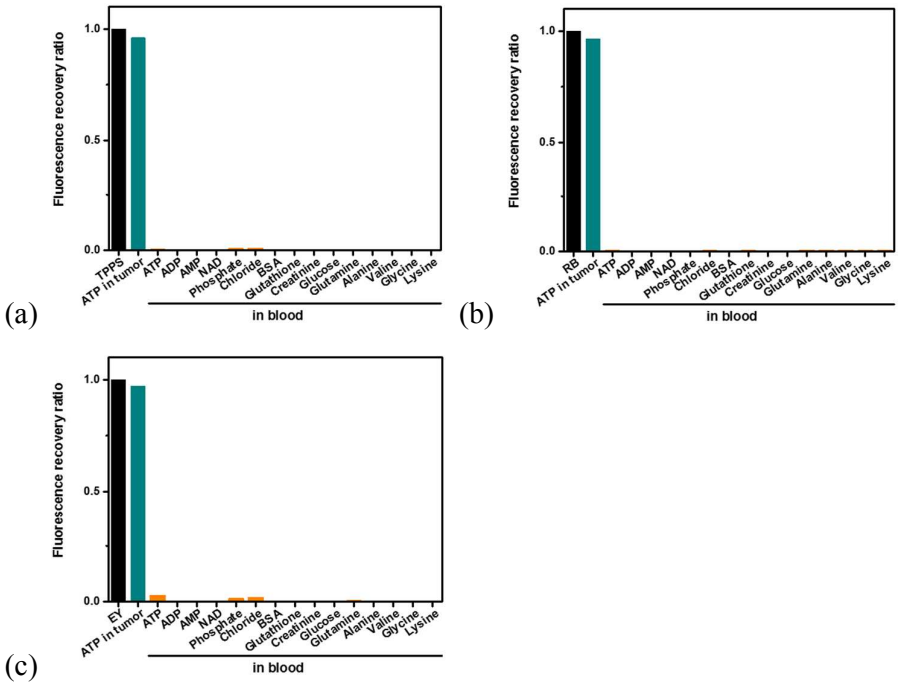

Figure S14. Fluorescence recovery of the PS/GC5A-12C nanoparticles (2.0/2.0 μM) upon addition of ATP and other components in blood in HEPES buffer (10 mM, pH = 7.4) at 25 °C, PS alone as control: (a) TPPS (λ_{ex} = 423 nm, λ_{em} = 644 nm), (b) RB (λ_{ex} = 550 nm, λ_{em} = 567 nm) and (c) EY (λ_{ex} = 517 nm, λ_{em} = 538 nm). Various biomolecules were added to the PS/GC5A-12C nanoparticle solutions and stirred for 30 min at 40 °C, then cooled to 25 °C to monitor the release of PS.

3.7 ATP-dependent $AlPcS_4$ release in cancer cells.

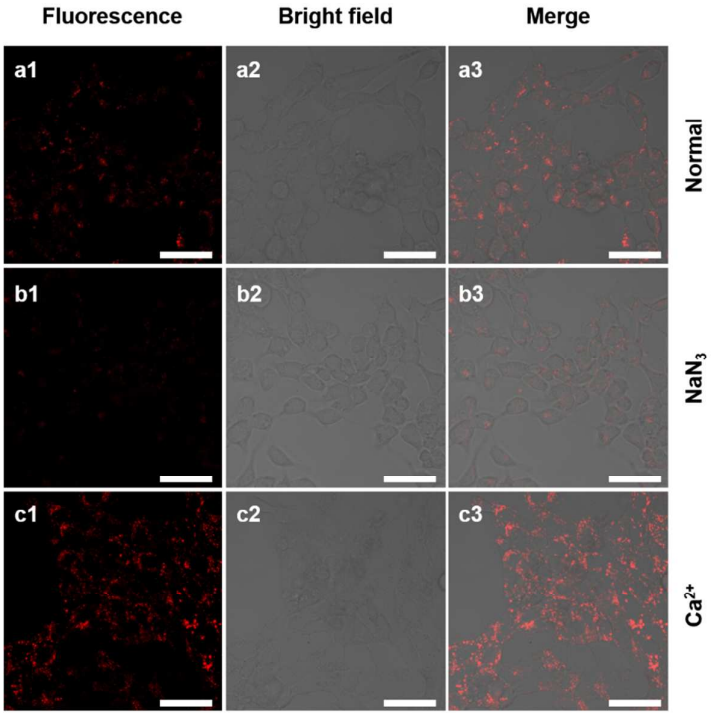

Figure S15. CLSM images of 4T1 cells after 6 h of incubation with (a) $AlPcS_4$/GC5A-12C (10/10 μM) in the absence, presence of (b) 10 mM of NaN_3 and (c) 5 mM of Ca^{2+}. Scale bar, 50 μm.

3.8 Intracellular $^1O_2$ detection.

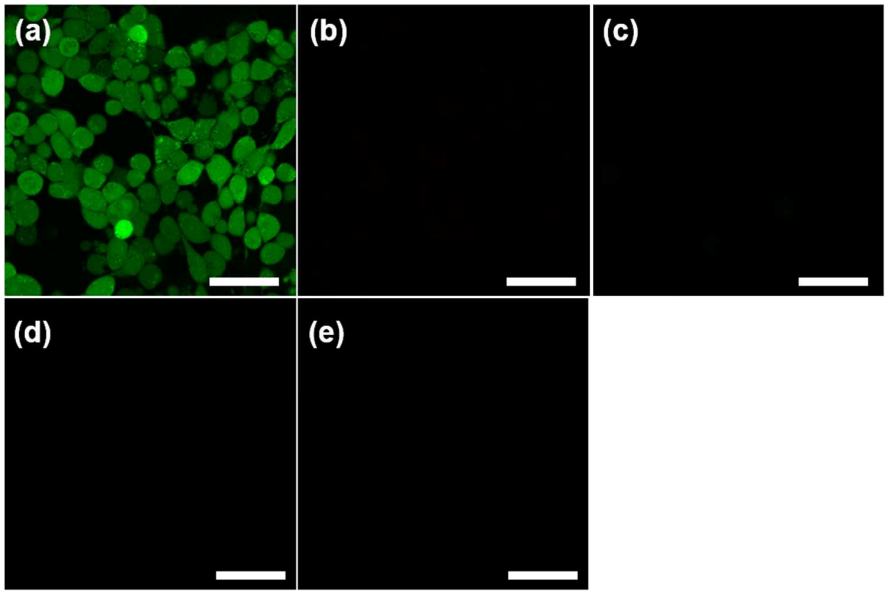

Figure S16. Intracellular $^1O_2$ detection by CLSM after 4T1 cells were treated with the $AlPcS_4$/GC5A-12C nanoparticle and DCFH-DA with 660 nm laser irradiation (a), no irradiation (b) and addition of N-acetylcysteine with 660 nm laser irradiation (c). Cells treated with DCFH-DA under irradiation (d) or dark (e) as control. Scale bar, 50 μm.

3.9 In vitro cytotoxicity assay of the GC5A-12C nanocarrier.

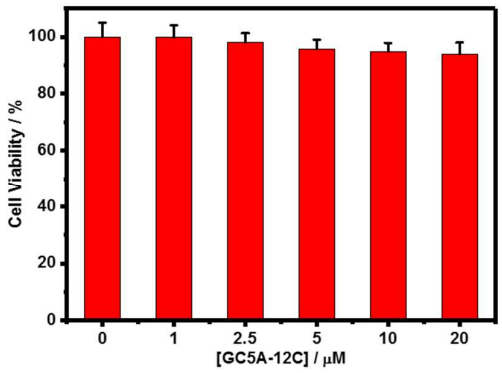

Figure S17. Cytotoxicity assay of the GC5A-12C nanocarrier against 4T1 cells. 4T1 cells were incubated with the GC5A-12C nanocarrier at different concentrations for 24 h, followed by cell viability assay. Error bars represent the standard derivations of three independent studies.

3.10 Intracellular PDT.

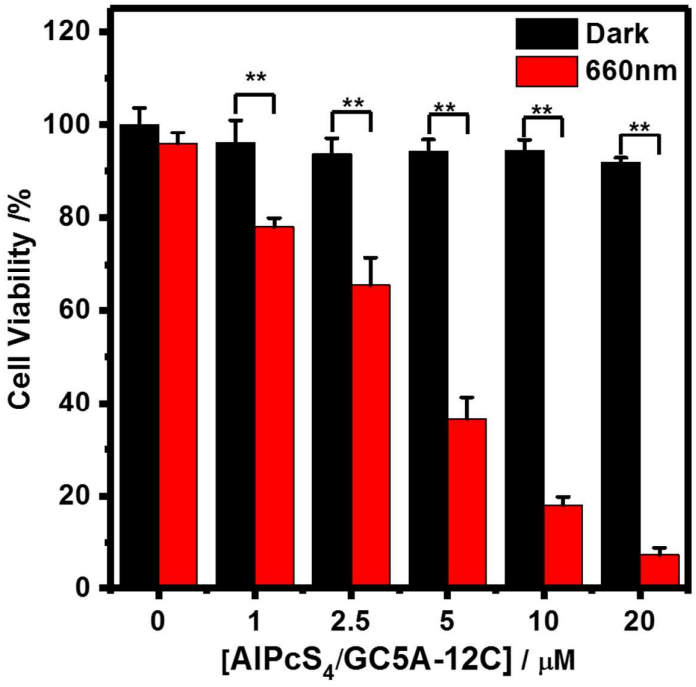

Figure S18. Cytotoxicity of the $AlPcS_4$/GC5A-12C nanoparticle against 4T1 cells in the absence (black) and presence of 660 nm laser irradiation (red). Cells without any treatment were used as control. $^{**}p < 0.01$. Error bars represent the standard derivations of three independent studies.

3.11 In vivo fluorescent imaging of mice *in situ* injected with the $AlPcS_4$/GC5A-12C nanoparticle and free $AlPcS_4$.

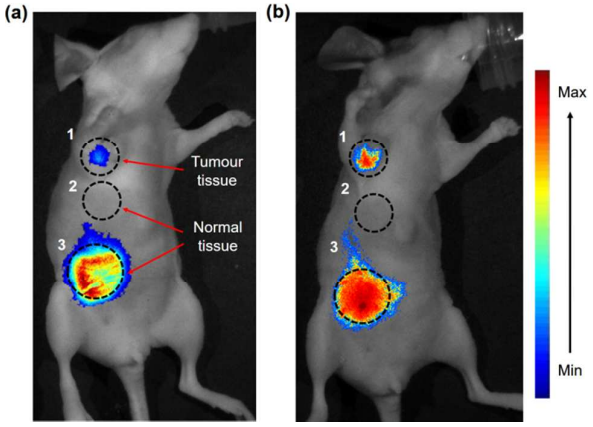

Figure S19. In vivo fluorescence imaging of the 4T1 tumour-bearing nude mice at 5 min (a) and 3 h (b) after *in situ* administration of the $AlPcS_4$/GC5A-12C nanoparticle

and free $AlPcS_4$. (1) the $AlPcS_4$/GC5A-12C nanoparticle was directly injected into tumour; (2) the $AlPcS_4$/GC5A-12C nanoparticle was subcutaneously injected into the normal skin; and (3) free $AlPcS_4$ was subcutaneously injected into the normal skin. $AlPcS_4$/GC5A-12C = 50/50 μM, at dose of $AlPcS_4$ 2.24 μg.

3.12 Histological H&E staining for spleen and liver.

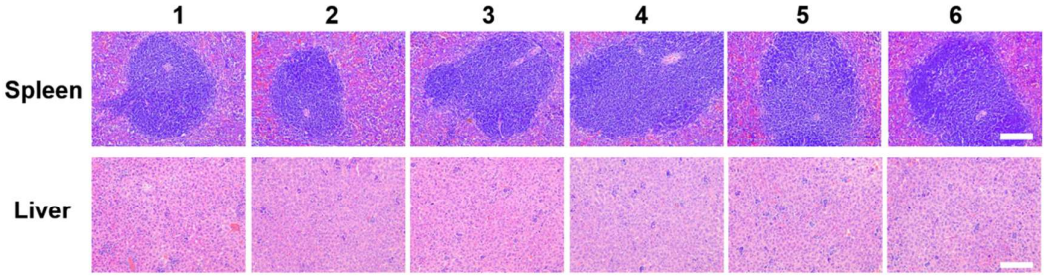

Figure S20. H&E staining for spleen and liver on day 16 after treatment. Scale bar is 100 μm. Group 1: Saline. Group 2: Saline 660 nm. Group 3: $AlPcS_4$. Group 4: $AlPcS_4$ 660 nm. Group 5: $AlPcS_4$/GC5A-12C. Group 6: $AlPcS_4$/GC5A-12C 660 nm.

References

(1) Geng, W.-C.; Liu, Y.-C.; Wang, Y.-Y.; Xu, Z.; Zheng, Z.; Yang, C.-B.; Guo, D.-S. *Chem. Commun.* **2017**, *53*, 392-395.

(2) Lakowicz, J. R. *Principles of Fluorescence Spectroscopy; Springer US*: New York, USA, 2006.

(3) Diéguez, L.; Darwish, N.; Mir, M.; Martínez, E.; Moreno, M.; Samitier. *J. Sensor Letters* **2009**, *7*, 851-855.

(4) Kraljić, I.; Mohsni, S. E. *Photochem. Photobiol.* **1978**, *28*, 577-581.

(5) Leonidova, A.; Pierroz, V.; Rubbiani, R.; Heier, J.; Ferrari, S.; Gasser, G. *Dalton Trans.* **2014**, *43*, 4287-4294.

(6) Dhami, S.; Cosa, J. J.; Bishop, S. M.; Phillips, D. *Langmuir* **1996**, *12*, 293-300.

(7) Harkness, R. A.; Coade, S. B.; Webster, A. D. B. *Clin. Chim. Acta 1984*, **143**, 91-98.

(8) Creeke, P. I.; Dibari, F.; Cheung, E.; van den Briel, T.; Kyroussis, E.; Seal, A. J. *J. Nutr.* **2007**, *137*, 2013-2017.

(9) Psychogios, N.; Hau, D. D.; Peng, J.; Guo, A. C.; Mandal, R.; Bouatra, S.; Sinelnikov, I.; Krishnamurthy, R.; Eisner, R.; Gautam, B.; Young, N.; Xia, J.; Knox, C.; Dong, E.; Huang, P.; Hollander, Z.; Pedersen, T. L.; Smith, S. R.; Bamforth, F.; Greiner, R.; McManus, B.; Newman, J. W.; Goodfriend, T.; Wishart, D. S. *PLoS ONE* **2011**, *6*, e16957.

(10) Ono, H.; Sakamoto, A.; Sakura, N. *Clin. Chim. Acta* **2001**, *312*, 227-229.

(11) Llewellyn, D. J.; Langa, K. M.; Friedland, R. P.; Lang, I. A. *Curr. Alzheimer Res.* **2010**, *7*, 91-96.

(12) Bowler, M. W.; Montgomery, M. G.; Leslie, A. G.; Walker, J. E. Proc. *Natl. Acad. Sci. USA* **2006**, *103*, 8646-8649.

(13) Griffiths, E. J.; Rutter, G. A. *Biochim. Biophys. Acta* **2009**, *1787*, 1324-1333.

(14) Arnaud-Neu, F.; Fuangswasdi, S.; Notti, A.; Pappalardo, S.; Parisi, M. F. *Angew. Chem., Int. Ed.* **1998**, *37*, 112-114.

(15) Garozzo, D.; Gattuso, G.; Notti, A.; Pappalardo, A.; Pappalardo, S.; Parisi, M. F.; Perez, M.; Pisagatti, I. *Angew. Chem., Int. Ed.* **2005**, *44*, 4892-4896.

(16) Zheng, Z.; Geng, W.-C.; Gao, J.; Wang, Y.-Y.; Sun, H.; Guo, D.-S. *Chem. Sci.* **2018**, *9*, 2087-2091.

(17) Scholz, M.; Dedic, R.; Breitenbach, T.; Hala, *J. Photochem. Photobiol. Sci.* **2013**, *12*, 1873-1884.

(18) Gandin, E.; Lion, Y.; Van de Vorst, A. *Photochem. Photobiol.* **1983**, *37*, 271-278.